

# **Effect of Scan Pattern on the Microstructural Evolution of Inconel 625 during Selective Laser Melting**

Md Ashabul Anam, JJS Dilip, Deepankar Pal, Brent Stucker  
Department of Industrial Engineering  
J.B Speed School of Engineering, University of Louisville, Louisville, KY 20292

REVIEWED

## **Abstract:**

Selective laser melting (SLM) involves highly localized heat input and directional solidification, which enables novel microstructure control through the development of scanning strategies and related process variables. A careful study of scan pattern is important to understand microstructural evolution during SLM. In this study, various types of scanning strategies were used to build samples of Inconel 625. Microstructure differences due to different scan patterns in as-built Inconel 625 samples were then studied in detail. Microstructure samples showed grains with cellular substructure with enriched regions of Nb and Mo in the inter arm spacing. The grains were observed to grow preferentially in the build direction, but there were also clear effects of grain orientation differences due to scan direction effects.

## **1. Introduction:**

Selective Laser Melting (SLM) is characterized by highly localized high heat input for very short periods of time, which has a profound impact on the microstructure. SLM provides a wide range of advantages over conventional manufacturing techniques, but high temperature gradients and rapid solidification cause high thermal stress build-up and the presence of non-equilibrium phases. Orientation of grains is largely controlled by the heat conduction direction, thus laser scanning strategy becomes a powerful tool for control of grain orientation, and hence the microstructural texture.

This paper focuses on the analysis of different scan strategies in order to obtain insight into the development of microstructural texture in Inconel 625 during SLM processing. It has been observed that SLM is a complicated process where the evolution of the microstructure depends on a large number of parameters such as laser power, scan speed, layer thickness, and scan strategy [1]. Most researchers have concentrated on the influence of process parameters on mechanical properties such as relative density, hardness and fatigue. From those studies, 20  $\mu\text{m}$  layer thickness was found to be optimal for In625 and for laser power and scan speed, a range of parameters were found to provide good mechanical properties. For the purpose of microstructural analysis, 20  $\mu\text{m}$  layer thickness and a 195W-800mm/s laser power-scan speed combination were primarily used. In this research two types of scanning strategies were investigated to understand their effects on the microstructures of IN625.

## 2. Scan Patterns in SLM

SLM machines typically utilize one of 2 basic scan strategies for the interior sections of parts. These strategies are either to scan the bulk of the part utilizing parallel stripes or by scanning the bulk of the part utilizing a block pattern.

### 2.1. Rotated Stripe Pattern

A schematic of a rotated stripe pattern is shown in figure 1. When using a stripe pattern, each layer is divided into a series of parallel stripes (red dashed line in figure 1) that run across the entire length of the cross-section of any closed contour within a layer. Within each stripe, raster scan vectors are used. During every new layer, the stripes rotate counterclockwise by  $\sim 67^\circ$  compared to the previous layer, creating a crosshatch pattern. Samples were cut from cylindrical fatigue specimens of diameter 10 mm and height 85 mm which were built in the Z direction in an EOS M270 machine using In625 powder from EOS (figure 2a). Both horizontal and vertical sections were taken and analysis was done using optical microscopy as well as scanning electron microscopy.

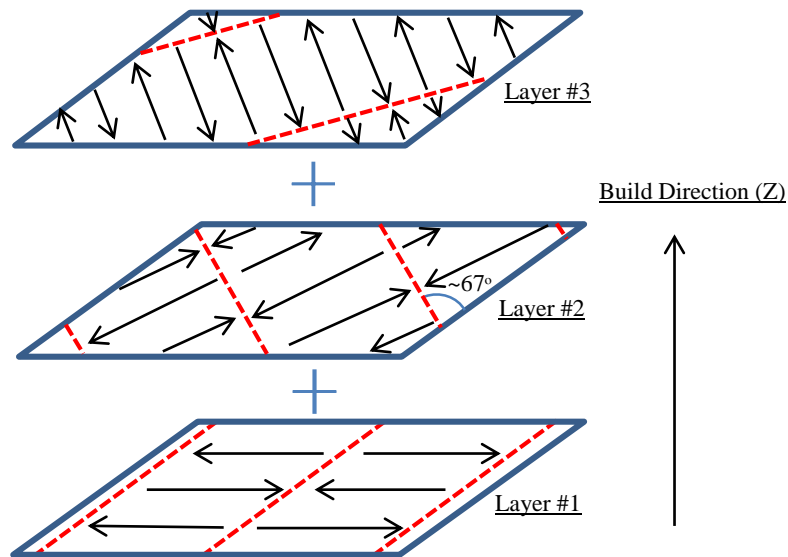


Figure 1: Schematic of a stripe scan pattern showing raster scan vectors (arrows) within each stripe (red dashed line). For every new layer, the stripes rotate by  $67^\circ$  compared to the previous layer.

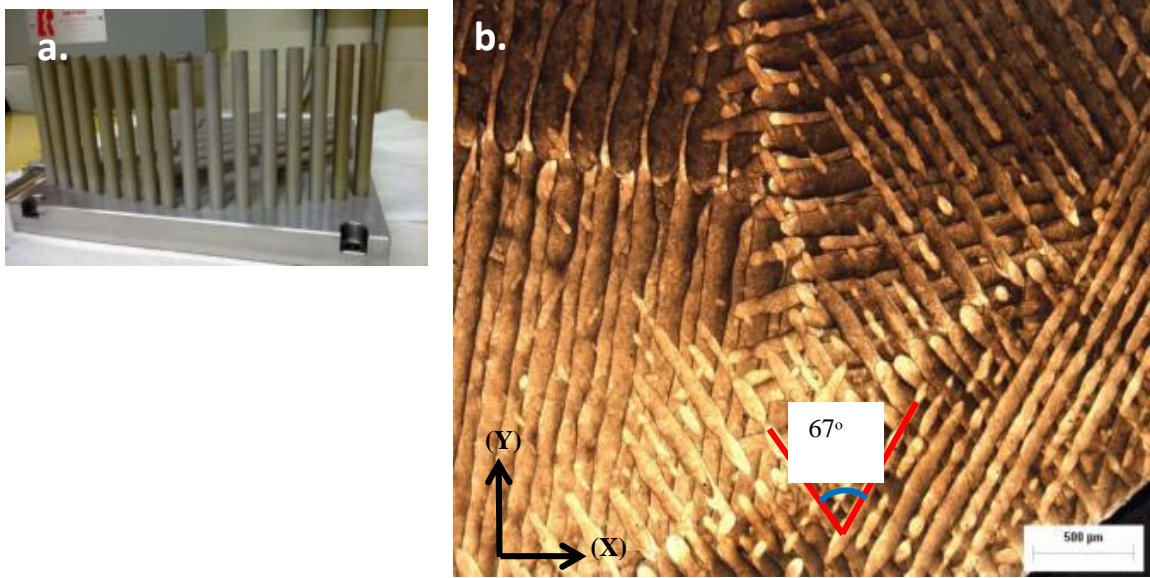


Figure 2: (a) Samples were cut from vertically built (Z orientation) cylindrical specimens. (b) Microstructural evidence of the stripe pattern, from a horizontal (XY plane) cross-section. Since the view plane is not perfectly horizontal, multiple layers intersecting the plane can be seen. The stripes rotate  $67^\circ$  for each new layer thus create a crosshatch patterns.



Figure 3: Melt-pool arrangement as seen from a vertical cross-section (YZ plane) for a stripe pattern.

In625 samples built using a rotated stripe scan strategy were etched and observed using optical microscopy. Figure 2(b) shows a vertical cross section of the sample where laser tracks are clearly distinguishable. The view plane in figure 2(b) is not perfectly horizontal (tilted slightly) which enables one to view multiple layers in the same image. The angle between laser tracks of consecutive layers was found to be  $67^\circ$  as illustrated in figure 1. Two stripes in the same layer, as well as their overlap, are visible in the top left corner of figure 2(b). In figure 3, the melt-pool arrangement in the vertical cross-section (YZ plane) is shown. It was observed that the shapes of

the melt-pools are quite similar (Gaussian) but their sizes are different. This is because scan vectors from different layers are not parallel to each other and not perpendicular to the view plane as well. Thus, different oblique sections of the melt-pools show different sizes.

## 2.2. Alternating Block Pattern

Schematics illustrating an alternating block scan strategy are shown in figure 4. In each layer, rectangular blocks with raster scan vectors are used and the scan vector rotates 90° between adjacent blocks. Between layers, the block shifts half of its width creating a “brick-like” stacking sequence. This scenario is clearly depicted in figure 4b where a schematic of a vertical cross-section (XZ plane) is shown (black circles represent scan vectors in the Y or -Y direction and black rectangles represent vectors in the X or -X direction). A block pattern such as this is typically designed to replicate the 0-90-0-90 stacking sequence often used in composites. However, the region labeled “Section A” in Figure 4b shows a stacking-based anomaly where a portion of that region has a 0-90-0-90 repeating structure and another portion of that same region has a 0-0-0-0 stacking sequence. Thin rectangular samples 2 mm thick, 40 mm long and 5 mm high were fabricated using In625 (figure 5) in an EOS M270 machine and analysis was done using optical microscopy as well as scanning electron microscopy to investigate this phenomena.

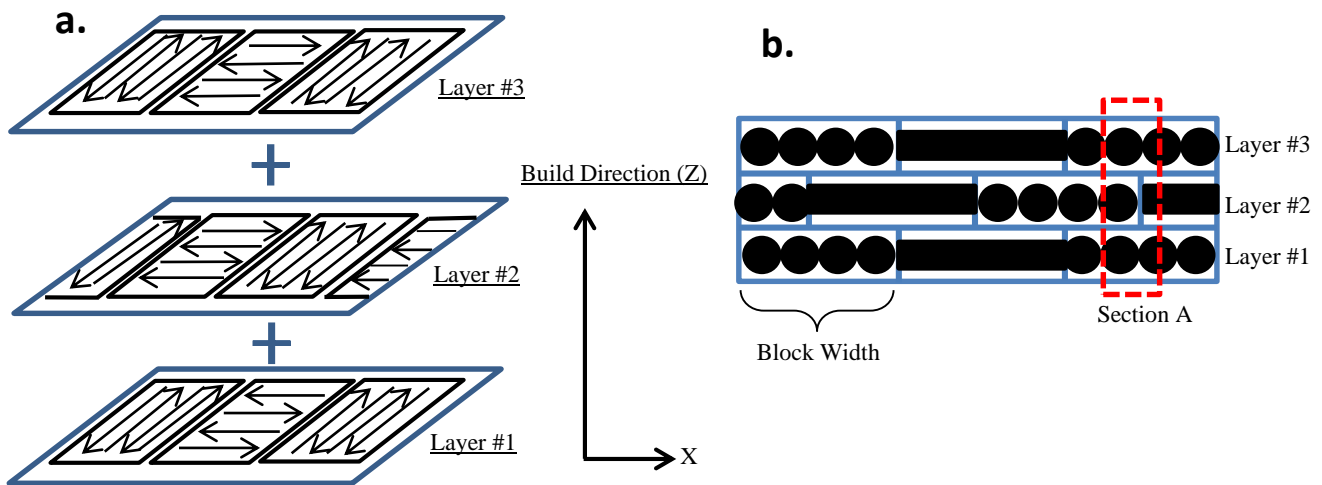


Figure 4: (a) Schematic of a block scan pattern showing raster scan vectors (arrows) within each block, (b) Vertical cross-section (XZ plane) showing scan line patterns between layers. In each new layer the block shifts half of its width.

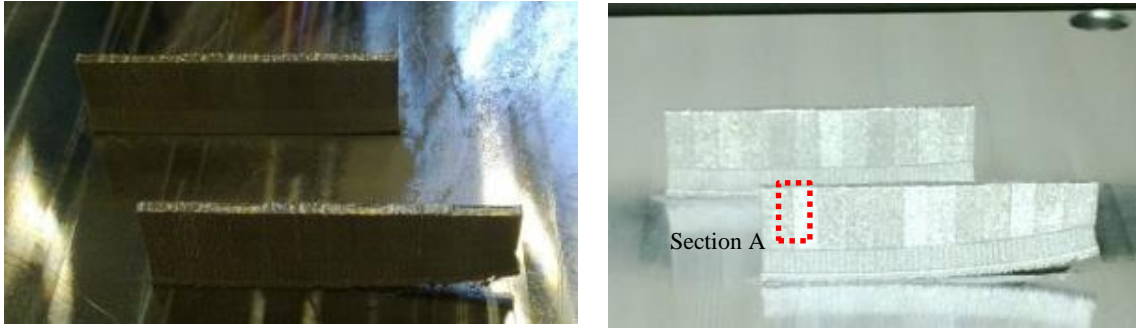


Figure 5: 40 mm x 5 mm x 2 mm blocks. Section A from the sample (Right) was cut and analyzed to understand the microstructural effects of the block scan strategy.

Section A from the sample in figure 5 was cut and polished and both vertical (XZ plane) and horizontal (XY plane) cross-sections were observed for microstructural features. Figure 6 shows the etched vertical cross section where melt-pool arrangement is clearly visible. The image can be separated into two distinct areas which were formed due to different scan vector overlaps. The left section of the image has a unidirectional melt-pool which were formed by blocks where all the scan vectors are parallel to each other for every layer (the direction was perpendicular to the view plane). The right section of the image shows scan vectors where layers create alternating hatch patterns. Section A of figures 4b and 5 illustrate how the pattern shown in figure 6 was created.

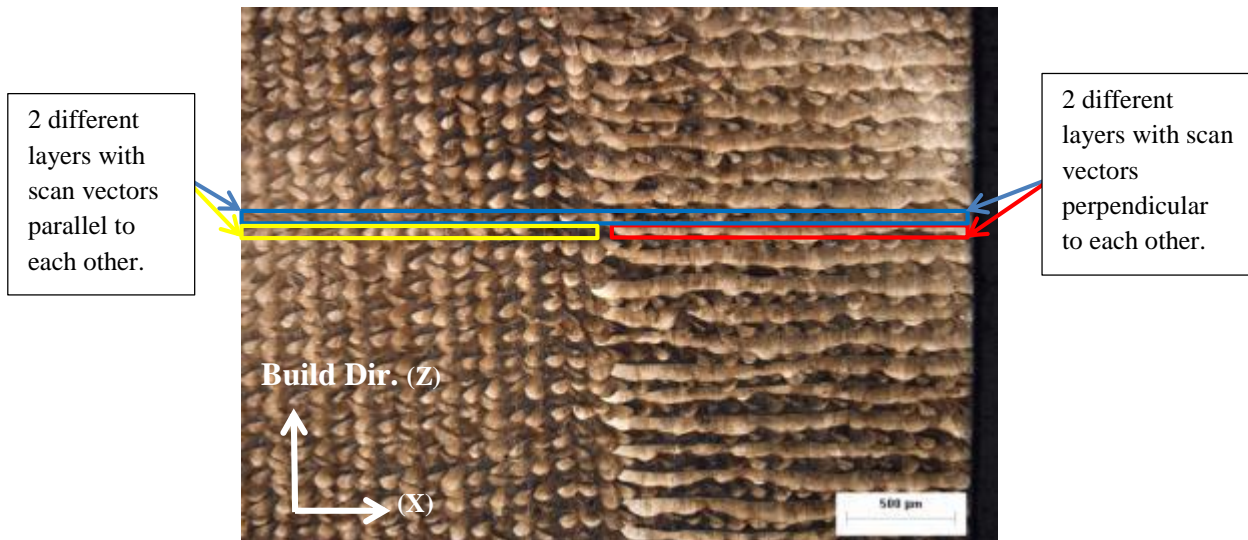


Figure 6: Melt-pool arrangement in a vertical cross-section (XZ plane) using a block pattern scan strategy.

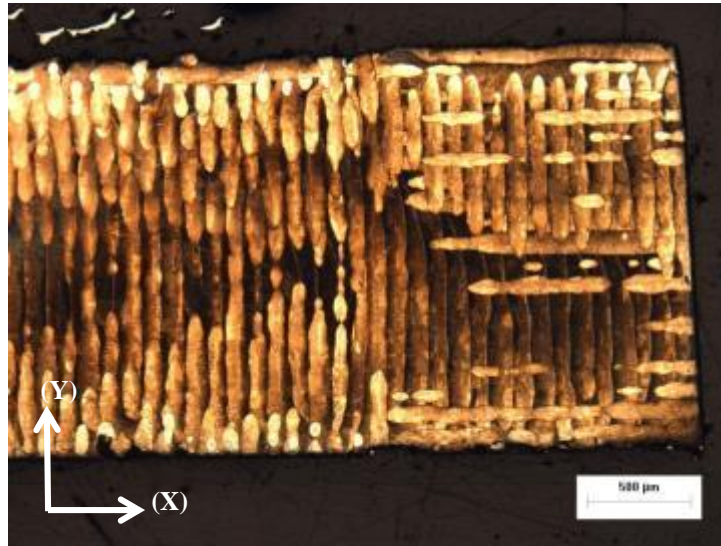


Figure 7: Block pattern, horizontal cross-section (XY plane) showing laser tracks for a block scan pattern. Since the view plane is not perfectly horizontal, multiple layers of laser tracks are seen.

### **3. Effect of Scan Pattern on Microstructure**

SLM is characterized by highly localized heat input for a very short period of time leading to rapid solidification as the melt pool undergoes liquid to solid transformations. This may result in formation of non-equilibrium phases and changes in general microstructural features. Finer cellular dendritic structures evolve due to high cooling rates compared to conventional manufacturing processes [2, 3, 8-11]. In addition, cellular/dendritic structures, and thus grain structures, are also controlled by microstructures formed at the boundaries of previously solidified layers (figure 8). Although the mechanism of grain growth is highly complex and influenced by many variables, local heat conduction direction plays an important role in determining the orientation of grains.

Temperature gradient is the highest along the midline of the scan track and at the back of the moving melt pool, and decreases radially [5]. Thus grains tend to grow in this direction (figure 8). However, due to overlap, major portions of laser tracks and their grains remelt during subsequent scanning. Due to the fast cooling conditions, the grains grow epitaxially toward the center of the new melt pool [4,6,7]. Based upon these conditions, the orientation of grains is thus highly dependent on the scanning velocity and scanning strategy. Consequently, the scanning strategy can become a powerful tool to control the grain orientation, and hence the microstructural texture [7,16,19,20].

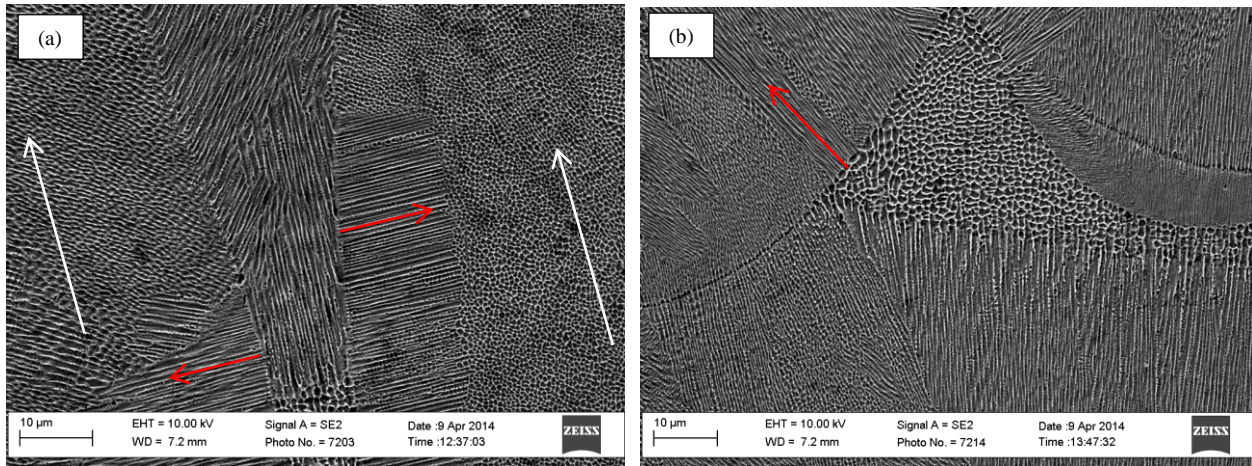


Figure 8: (a) SEM image of a horizontal (XY) section showing cellular/dendritic growth (red arrows) towards the center of the scan track (white arrow), (b) vertical (YZ) section showing radial growth of cellular dendrites. Clear melt-pool boundaries are observed which has an effect on grain size and orientation.

Thijs et. al. (2010) studied different scan strategies for Ti-6Al-4V and found that grains grow preferentially in the build direction. They reported that elongated grains are parallel to each other and are tilted at an angle  $19^\circ$  away from building direction for a unidirectional scan pattern. For bidirectional and grid-like scan patterns (figures 6 and 7), elongated grains were found to grow preferentially in the build direction (figure 9b).

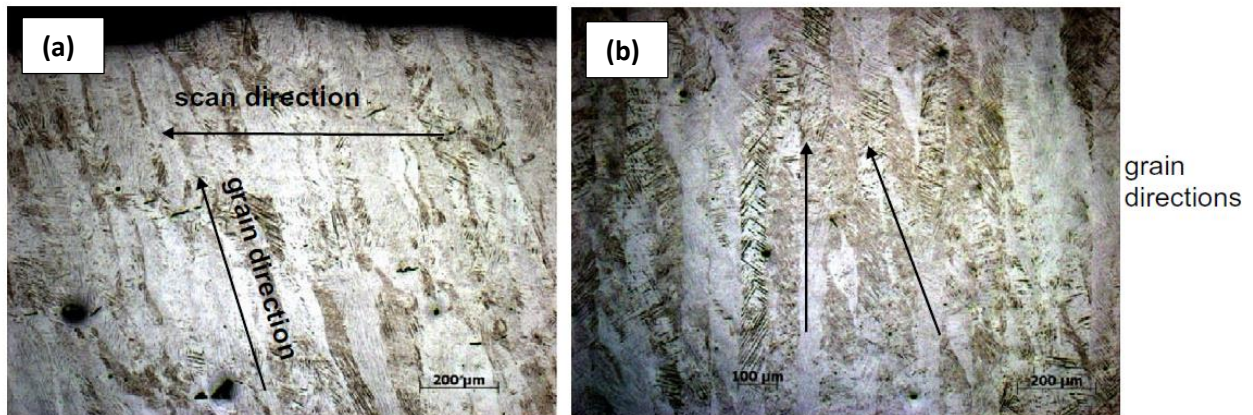


Figure 9: Orientation of elongated grains scanned with: (a) unidirectional scan vectors, and (b) alternating hatch scan vectors. View plane: Side view (YZ plane), Material: Ti-6Al-4V. [7]

Similar phenomena were observed for In625. For a stripe scan strategy which rotates  $67^\circ$  for every new layer, more refinement of cellular/dendritic structures occurs due to maximum overlap in the melt, creating more elongated grains. Figure 10 shows optical microscopy of elongated grains oriented in the build direction (Z).

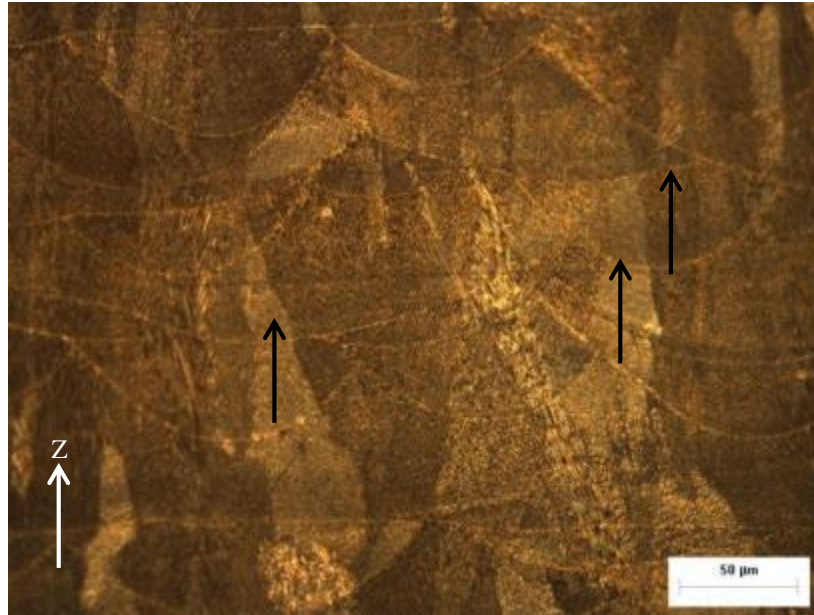


Figure 10: Orientation of elongated grains (dark and white regions) formed due to the stripe pattern, which grow preferentially in the build direction (z) indicated by black arrows across multiple layers.

Despite epitaxial solidification, melt pools are still distinguishable due to the appearance of dark bands in optical microscopy (white bands in SEM) (figure 11). These dark bands are more noticeable when more energy is applied. The dark contrast which distinguishes these bands arises due to enhanced precipitation of Nb and Mo which are preferentially etched [2,3,12-15]. EDS analysis was done for this identification and is shown later in this paper.

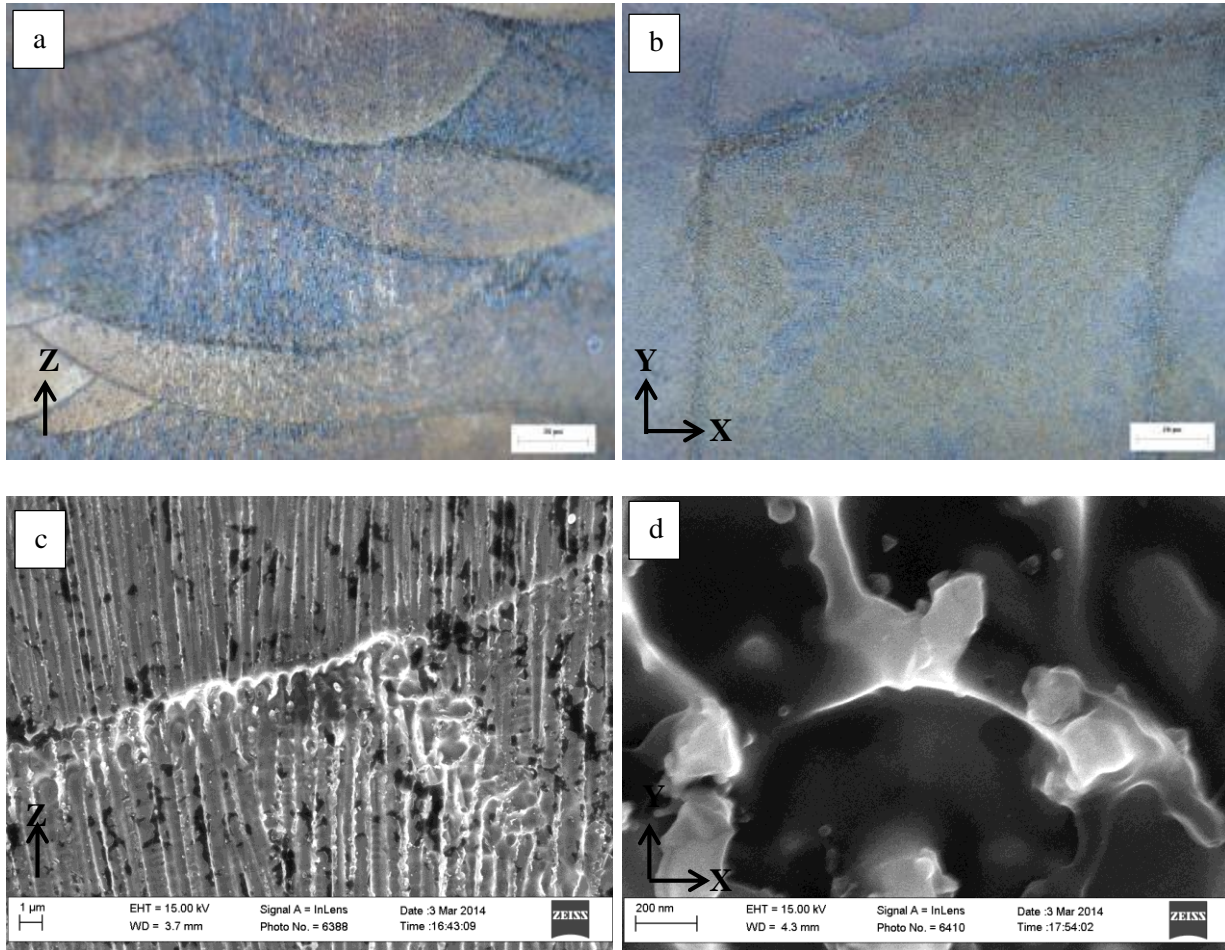


Figure 11: (a) Optical microscopy showing a vertical section of In625 where melt pools are distinguishable due to the appearance of dark bands. (b) Horizontal section showing dark band region. (c) SEM image showing the same section as ‘a’ but magnified to illustrate that SEM white regions represent optical microscopy dark bands. (d) High magnification SEM image of a horizontal section showing the cross-section of a single dendrite where the white region is formed due to segregation of Nb and Mo.

Figure 12(a) shows a typical polished and etched SEM micrograph of the vertical cross-section of an In625 part built using a rotated stripe pattern. It can be observed from the micrograph that the grains have grown epitaxially and there is grain continuity across multiple melt pools in the build direction. The columnar grains show cellular and dendritic sub-structure. It can also be observed that there is noticeable segregation (bright regions) within the intercellular and interdendritic arm spacing. Intercellular spacing is less than 1  $\mu\text{m}$  (figure 13) which provides excellent strength and hardness that can be achieved both in the as processed and aged conditions.

Figure 12(b) shows a typical polished and etched SEM micrograph of the vertical cross-section of an In625 SLM sample using a block scan pattern. The microstructural features show epitaxial grain growth from the melt. The grains show columnar morphology with a cellular / dendritic sub-structure. The individual cell/dendrite boundaries are illuminated by segregation of elements during solidification into the inter cell/ dendritic arm spacing. There is also grain continuity across multiple melt pools, which is also common for multipass welds of this alloy. For alternating scan patterns, the elongated columns were found to have shorter length compared to rotated stripe patterns.

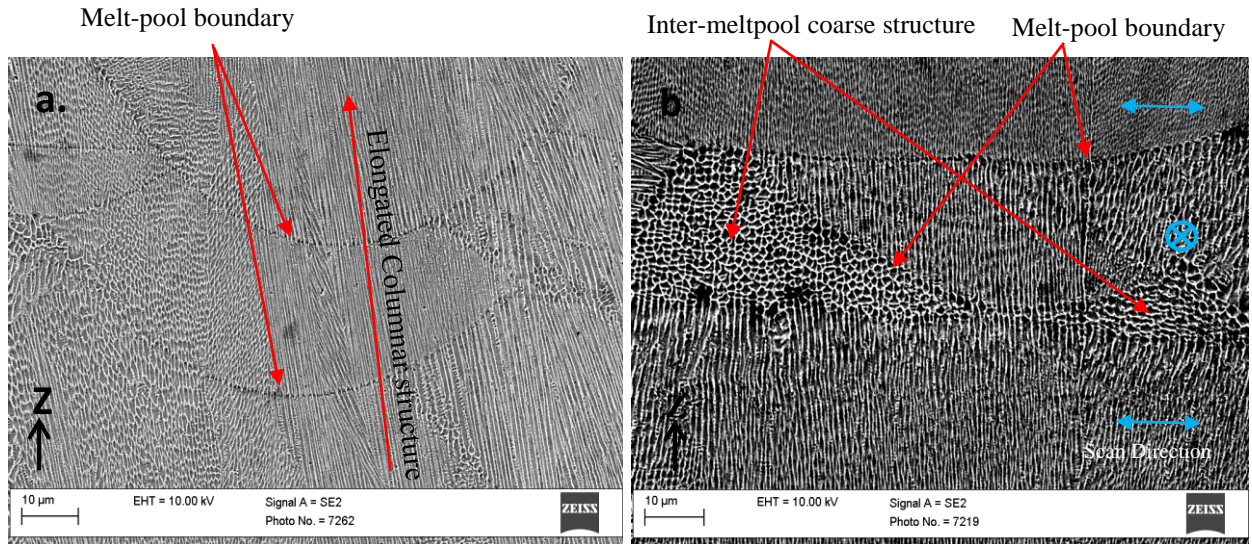


Figure 12: SEM image showing vertical cross-section (YZ plane) of In625 sample built using (a) rotated stripe pattern and (b) alternating block pattern. Arrows in the right section in ‘b’ show alternating scan directions.

Another distinguishable feature is that regions of coarse columnar structure appear in between melt pools in figure 12(b). These regions are less refined. Refinement in columnar structure is done by laser re-melting which is reported by several authors [10,17]. Melt-pool depth for this experiment is approximately 60 µm, which influences three layers. Therefore overlap and remelting become a common phenomenon in SLM processing. However alternating block patterns leaves a significant amount of inter-meltpool regions which are not overlapped. These inter-meltpool regions undergo incipient melting, developing a continuous network of undesirable interdendritic phase. For rotated stripe patterns, higher overlap and thus finer cellular structure is found. Cellular structure size and direction have significant effect on material strength. Finer structures provide higher hardness and good fatigue strength [18].

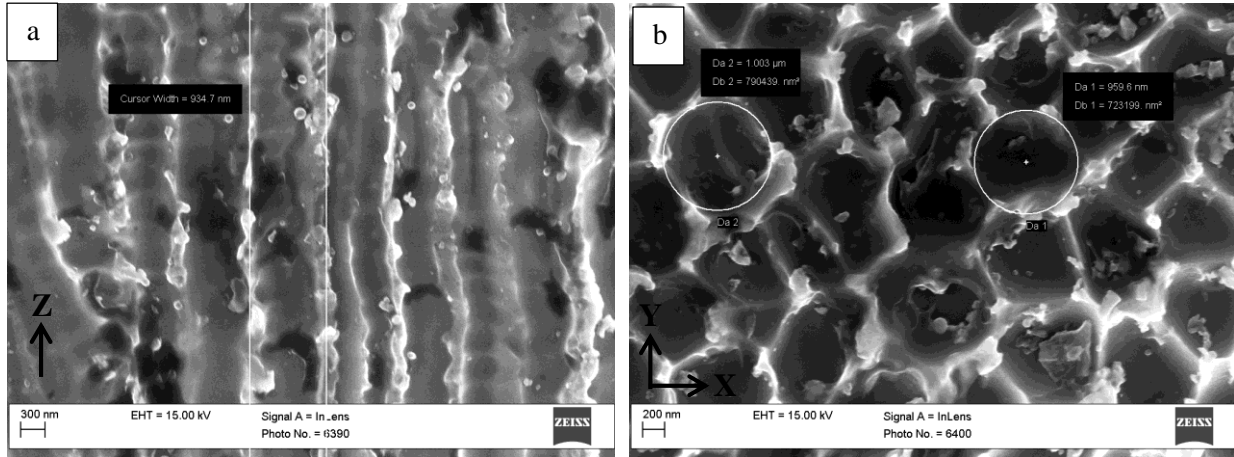
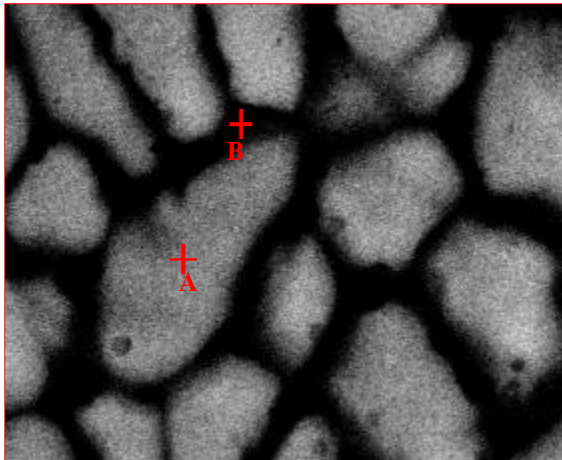


Figure 13: SEM image showing intercellular spacing less than 1  $\mu\text{m}$  for a rotated stripe scan pattern in (a) vertical and (b) horizontal sections, which provide excellent strength and hardness.

#### 4. EDS Analysis

Local chemical composition of the cell/dendrites and within inter cell / dendritic arms was evaluated qualitatively by using energy spectroscopy in SEM. The inter cell / dendritic regions show regions enriched in Nb and Mo.



Position	Material Composition (Wt. %)			
	Nb	Mo	Cr	Ni+Others
Point A: On Matrix	2.04	5.62	18.06	74.29
Point B: On Column Boundary	3.34	6.31	17.82	72.53

Figure 14: EDS spectrum comparison for two different points showing enriched Nb and Mo in dendritic arms boundaries.

## **5. Backscattered Electron Imaging**

The samples were also observed in the BSE mode in SEM. The BSE imaging mode gives the atomic number contrast of elements in the microstructure under observation. The BSE SEM micrograph of the vertical cross section further confirms the segregation of elements in the intercell/dendritic arm regions.

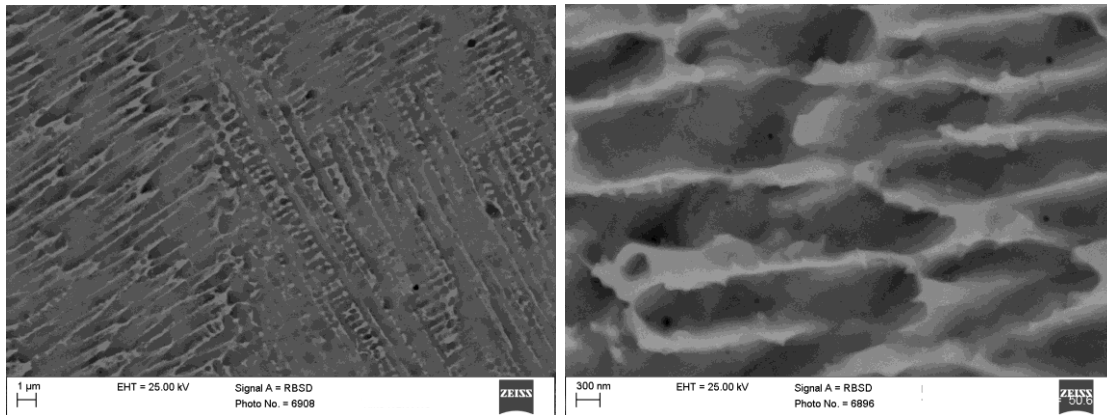


Figure 15: BSE image of a vertical (YZ) cross-section at two different magnifications.

## **6. Summary**

Two types of scan patterns were analyzed in detail using schematics as well as optical and SEM microscopy for In625 samples fabricated using selective laser melting. A rotated stripe pattern which uses raster scan vectors and which rotates  $\sim 67^\circ$  for every new layer creates a crosshatch pattern. A block pattern, on the other hand, uses raster scan vectors in each block and shifts half of its width between each new layer, thus creating brick-like building blocks and regions where no shift in scan vectors occur.

In SLM, local thermal gradients inside the melt pool are the most important factor for determining microstructure. The heat conduction direction, based upon scan pattern, plays an important role in determining the orientation of grains. Solidification occurs in a cellular/dendritic fashion with the growth direction preferably oriented towards the center of the melt pool. However, due to overlap, major parts of each solidified track remelts and the grains grow epitaxially towards the center of the new, adjacent melt pool. Microstructures of previously solidified layers also control the direction of cellular/dendritic growth.

Noticeable amounts of segregation within the intercellular and interdendritic arms spacing were observed. Intercellular spacing is less than 1  $\mu\text{m}$ , which contributes to the excellent strength and hardness that can be achieved both in as-processed and aged conditions. These cells are not individual grains but constitute a substructure inside one grain.

Grains grow epitaxially and there is grain continuity across multiple melt pools in the build direction. However, for an alternating block pattern, the elongated columns are found to have shorter length compared to a rotated stripe pattern.

Difference in cellular structure were observed in alternating block patterns. Inter-melt pool regions undergo incipient melting, developing a continuous network of undesirable interdendritic phase, thus resulting in coarse cellular structures which should affect hardness and strength significantly.

### **Acknowledgement**

The authors would like to thank the staff at the University of Louisville Rapid Prototyping Center for help with fabrication of test coupons. The authors also acknowledge support of the National Institute of Standards and Technology (NIST), through a collaboration grant (Number 70NANB12H262). NIST DMLS facilities were used to fabricate the cylindrical test bars.

### **References**

- [1] Anam Md, Pal D., Stucker B., Modeling and Experimental validation of Nickel-based super alloy (Inconel 625) made using Selective Laser Melting. SFF Symposium 2013 proceedings. Page: 463-473.
- [2] Amato KN, Gaytan SM, Murr LE, Martinez E, Shindo PW, Hernandez J, et al. Microstructures and mechanical behavior of Inconel 718 fabricated by selective laser melting. *Acta Mater* 2012;60:2229-39.
- [3] Amato KN, Hernandez J, Murr LE, Martinez E, Gaytan SM, , Shindo PW, Comparison of Microstructures and Properties for a Ni-Base Superalloy (Alloy 625) Fabricated by Electron and Laser Beam Melting. *Journal of Materials Science Research* 2012; 1:5539-39
- [4] Vrancken B, Wauthle R., Kruth JP, Humbeeck JV, Study of the Influence of Material Properties on Residual Stress in Selective Laser Melting. *Proceedings of SFF Symposium*, page:393
- [5] Alimardani M, Toyserkani E, Huissoon JP, Paul CP. On the delamination and crack formation in a thin wall fabricated using laser solid freeform fabrication process: An experimental--numerical investigation. *Opt Lasers Eng* 2009;47:1160-8.
- [6] Kruth JP, Deckers J, Yasa E, Wauthle R. Assessing and comparing influencing factors of residual stresses in selective laser melting using a novel analysis method. *Proc Inst Mech Eng Part B-J Eng Manuf* 2012;226:980-91.
- [7] Thijs L, Verhaeghe F, Craeghs T, Van Humbeeck J, Kruth JP. A study of the micro structural evolution during selective laser melting of Ti-6Al-4V. *Acta Mater* 2010;58:3303-12.
- [8] Murr LE, Quinones SA, Gaytan SM, Lopez MI, Rodela A, Martinez EY, et al. Microstructure and mechanical behavior of Ti-6Al-4V produced by rapid-layer manufacturing, for biomedical applications. *Journal of the Mechanical Behavior of Biomedical Materials* 2009;2:20-32.
- [9] Kelly S, Kampe S. Microstructural evolution in laser-deposited multilayer Ti-6Al-4V builds: Part I. Microstructural characterization. *Metall Mater Trans A* 2004;35:1861-7.
- [10] Kruth JP., Badrossamay M., Yasa E., Deckers J., Thijs L., Humbeeck J.V., Part and Material

Properties in Selective Laser Melting of Metal. Proceedings of the 16th International Symposium on Electromachining 2010.

[11] Shankar, V., Rao, Shankara, Mannan, S.L., Microstructure and Mechanical Properties of Inconel 625 Superalloy. *Journal of Nuclear Materials* 288 (2001) 222-223.

[12] Metallography of Superalloys, G.F. Vander Voort, Buehler Ltd., October 2003

[13] Metals Handbook Ninth Edition, Volume 9, pp. 305 – 309 . ASM International, Materials Park, OH. 1985

[14] Starr T.L., Rafi K., Stucker B., Scherzer C.M. (2012). “Controlling phase composition in selective laser melted stainless steels.” Proceedings of 2012 Solid Freeform Fabrication Symposium, the University of Texas, Austin.

[15] Paul, C.P, Ganesh, P., Mishra, S.K., Bhargava, P., Negi, J., Nath, A.K., “Investigating laser rapid manufacturing for Inconel-625 components” *Journal of Optics & Laser Technology* 39 (2007) 800–805.

[16] Gibson, I., Rosen, D.W., and Stucker, B. *Additive Manufacturing Technologies: Rapid Prototyping to Direct Digital Manufacturing*. Springer, 2009.

[17] Kruth, J.-P., Deckers, J., Yasa, E., 2008, experimental investigation of laser surface remelting for the improvement of laser melting process, Proc. SFF Symp., Austin, Texas, USA, 321-322

[18] Simchi, A., Pohl, H., 2003, Effects of laser sintering processing parameters on the microstructure and densification of iron powder, *Materials Science and Engineering A* 359: 119-128.

[19] Yasa, E., Kruth, J.-P., 2009, Microstructure evolution of selective laser molten 316L stainless steel parts with laser re-melting, Proc. 5th Int. WLT-Conference on Lasers in Manufacturing (LIM), Munich, Germany

[20] Rombouts, M., Froyen, L., Bourell, D.L., Kruth, J.-P., 2005, Roughness after laser melting of iron based powders, Proc. 2nd Int. Conf. on Advanced Research in Virtual and Rapid Prototyping VRAP, Leiria, Portugal, 329-335